



Physical Interpretation of Interwell Partitioning Tracer Tests for Estimation of Remaining Oil Saturation in Layered Carbonate Reservoirs

Samuel D. Fontalvo¹ · Maxim P. Yutkin¹ · S. Majid Hassanizadeh^{2,3} · Clayton J. Radke⁴ · Tadeusz W. Patzek¹

Received: 30 May 2025 / Accepted: 4 June 2025
© The Author(s) 2025

Abstract

Interwell partitioning tracer tests (IPTTs) are conducted in mature oil fields to estimate remaining oil in place, which is crucial for subsequent economic analyses and decisions regarding further field development. An IPTT involves the simultaneous injection of two types of tracers: conservative and partitioning, that probe the aqueous and oil phases, respectively. Although this test requires time, it probes the entire fluid flow path, not just the near-wellbore area, as is the case with other methods such as single-well tests. Accurate interpretation of interwell tracer test data is of critical importance for the oil and gas industry. Published IPTT case studies lack physical justification for the choice of tracer flow models. In this study, we provide such justifications along with guidelines for selecting appropriate tracer flow models. First, we review existing models for the transport of partitioning and conservative tracers and demonstrate their applicability range based on mass conservation analysis. Based on this analysis, we propose a refined model of partitioning tracer flow with Robin boundary conditions that accounts for non-equilibrium partitioning. Such analysis is missing in the literature. Next, we illustrate errors in estimating remaining oil if an inappropriate model is used for data interpretation. Notably, the choice of an incorrect model can lead to either underestimation or overestimation of the remaining oil, with the latter being of greater financial concern. Finally, we apply the non-equilibrium partitioning model to a published IPTT dataset from a layered carbonate reservoir and compare our remaining oil estimates with results of the original study. To the best of our knowledge, analysis of such cases with non-equilibrium partitioning has not been documented in the literature.

Keywords Diffusion limited partitioning · Boundary conditions · Non-equilibrium partitioning · Mass-balance analysis

List of Symbols

α	Diffusive mass-transfer rate coefficient (T^{-1})
a_V^i	Specific surface area of oil-brine interface (L^{-1})
C_w	Tracer concentration in the water phase ($M L^{-3}$)
C_o	Tracer concentration in the oil phase ($M L^{-3}$)

Extended author information available on the last page of the article

C_{init}	Initial tracer concentrations (M L^{-3})
C_{inj}	Injected tracer concentrations (M L^{-3})
$\tilde{C}(x, t)$	Dimensionless tracer concentration (–)
D_{H}	Hydrodynamic dispersion coefficient in the longitudinal direction ($\text{L}^2 \text{T}^{-1}$)
D_{m}^{o}	Partitioning tracer molecular diffusion coefficient in the oil ($\text{L}^2 \text{T}^{-1}$)
δ	Average characteristic dimension of oil blobs or patches (L)
Da_{m}	Mass transfer Damköhler number (–). Given by $\text{Da}_{\text{m}} = a_{\text{v}}^i D_{\text{m}}^{\text{o}} L / \delta v$
K	Partitioning coefficient (–), given by $K = C_{\text{o}} / C_{\text{w}}$
L	Characteristic macroscopic length of the domain (m). Distance between inlet/injection and outlet/production of the solute
ϕ	Fluid-accessible porosity (–)
Pe_{L}	Longitudinal Péclet number (–). Given by $\text{Pe}_{\text{L}} = vL / D_{\text{H}}$
R	Retardation factor (–). Given by $R = 1 + KS_{\text{o}} / S_{\text{w}}$
r^{wo}	Rate of mass transfer from water to oil phase ($\text{M L}^{-3} \text{T}^{-1}$)
S_{w}	Water saturation (–)
S_{o}	Oil saturation (–)
t_{s}	Injected slug/pulse time (T)
t_{b}	Breakthrough time or mean residence time (T). Given by

$$t_{\text{b}} = \frac{\int_0^{\infty} C(x = L, t) dt}{\int_0^{\infty} C(x = L, t) dt} - t_{\text{s}}/2$$

t_{b}^{p}	Arrival time of the partitioning tracer (T)
t_{b}^{c}	Arrival time of the conservative tracer (T)
\tilde{t}	Dimensionless time or pore volumes (–). Given by $\tilde{t} = vt / L$
u	Superficial (Darcy) velocity (L T^{-1})
v	Interstitial velocity, given by $v = u / \phi S_{\text{w}}$
\tilde{x}	Dimensionless distance (–). Given by $\tilde{x} = x / L$

1 Introduction

In the oil and gas industry, tracer tests are used to determine fluid-accessible pore volume, dispersivity of a porous medium, reservoir heterogeneity, connectivity between wells, and most importantly, to estimate remaining oil saturation—a tool that enables improved/enhanced oil recovery projects (Brigham and Smith 1965; Cooke 1971; Shook et al. 2009; Tang and Harker 1991a; Dwarakanath et al. 1999; Maroongroge 1994; Hartvig et al. 2015; Viig et al. 2013; Huseby et al. 2015). In general, two approaches are available: single-well and interwell tests. The former involves injecting and producing dissolved tracer into and from the same well, whereas the latter uses separate wells for injection and production. The advantages and drawbacks are straightforward: single-well tests are fast but probe only small near-wellbore regions, whereas interwell tests take a long time (up to years) but provide a more comprehensive picture. Although some applications can benefit from fast single-well test results, accurate estimation of remaining oil for informed business decisions favors the use of interwell tests.

To determine oil saturation, two types of tracers should be injected simultaneously into the formation: one conservative, which stays only in the aqueous phase, and one

partitioning, which can partition between phases. As such tests are typically performed at a mature phase of waterflooding, the oil phase is likely mostly stagnant.

In an interwell tracer test, a small amount of an inert chemical (i.e., conservative tracer) is dissolved in aqueous phase and injected into the porous medium at an injection point and then is advected toward the outlet. The effluent is continuously collected at the outlet or producer well and analyzed for the inert chemical content. The resulting concentration breakthrough curve (i.e., concentration vs. time or pore volumes) of the conservative tracer carries information about the pore space and flow paths of the porous medium. Moreover, the conservative tracer serves as an arrival time reference for all other reactive (i.e., non-inert) chemical species that may have been injected along with the tracer or originated from the porous medium.

Partitioning tracers are chemicals that can partition from the aqueous phase into the oil phase. Typically, partitioning tracers are bulky organic molecules, and their transport depends on several factors, such as advection and dispersion in the mobile phase, as well as the partitioning and diffusion coefficients in the oil phase (Cooke 1971). There are two options for describing the partitioning of the tracer between the two phases: equilibrium (fast) partitioning characterized by a linear partitioning coefficient, and mass transfer-limited (slow) partitioning that in the limit reaches the linear equilibrium conditions and is characterized by a mass transfer coefficient.

The mass transfer-limited partitioning problem is physically very similar to flow and transport in saturated or unsaturated porous media with stagnant zones. In the literature, there are two advection–dispersion models with stagnant zones that describe both fast and slow diffusion into the stagnant zones (Deans 1963; Coats and Smith 1964; Rao et al. 1980a, b; Genunchten and Wierenga 1976; Skopp and Warrick 1974). Deans (1963) presented a dual-zone diffusion model with mass transfer into the stagnant zone. This model assumes that a mass transfer coefficient accounts for solute transport in and out of the stagnant zone, and the driving force for transport into the stagnant zone is a pore-scale concentration gradient. Coats and Smith (1964) extended this model to account for advection, which is appropriate for typical reservoir operating conditions. More recently, Niessner and Hassanizadeh (2009) derived an interphase kinetic mass transfer model from thermodynamic principles and included the specific interfacial area as a model parameter.

However, such models are not precisely equivalent to partitioning tracer transport with stagnant oil because the physico-chemical processes are different. In the stagnant zones model, mass transfer occurs between mobile and immobile zones of the same fluid, so the driving force is only the concentration difference within the same phase. In the partitioning tracer transport with stagnant oil model, mass transfer occurs between mobile and immobile zones of different fluids. The driving force is the concentration difference between phases and is characterized by a linear equilibrium partitioning coefficient, which defines the distribution of the partitioning tracer in the phases.

If the partitioning of the tracer into the stagnant oil phase occurs rapidly, the equilibrium partitioning model is sufficient. Raimondi and Torcaso (1965) conducted coreflooding experiments with conservative and partitioning tracers. In their experiments, despite increased flow velocity, all experiments appeared to be under equilibrium conditions. So, experimental evidence suggests equilibrium partitioning under broad experimental conditions. However, reservoir-scale processes differ substantially from lab-scale experiments, so the equilibrium assumption may not hold. The transport equation for equilibrium partitioning conditions is identical to that of adsorptive transport with a retardation factor. In the partitioning tracer case, however, the retardation factor depends on the remaining oil saturation (Genunchten 1981; Nkedi-Kizza et al. 1984). Indeed, Cooke (1971) patented

a method to estimate remaining oil saturation simply from the arrival times of conservative and partitioning tracers, based on equilibrium partitioning. Cooke's approach has been widely used in industry to estimate remaining oil.

More importantly, most, if not all, published analyses of interwell partitioning tracer tests assume fast equilibrium of the partitioning tracer with the oil phase. Non-equilibrium conditions are not considered explicitly (Hartvig et al. 2015; Viig et al. 2013; Huseby et al. 2015; Sanni et al. 2016). Some Lattice Boltzmann formulations incorporate tracer partitioning physics implicitly (Berkowitz et al. 2008; Khirevich and Patzek 2019). However, to our knowledge, no published continuum models describe tracer flow with non-equilibrium partitioning into stagnant oil, with the partitioning defined by a partitioning coefficient and governed by a mass transfer rate.

The interpretation of conservative tracer data relies on the solution of the advection–dispersion equation (ADE). Although reservoirs are 3D structures, most, if not all, published interpretations of partitioning tracer tests are based on 1D models (Brigham and Smith 1965; Tang and Harker 1991a, b; Viig et al. 2013; Sanni et al. 2016). However, as we show below, even applying 1D models for tracer data interpretation is challenging. A thorough understanding of a simplified 1D case serves as a basis for more complex and precise 3D reservoir descriptions. Several studies address stratified reservoirs with layers of varying permeability. In 1D modeling, tracer data from such reservoirs can typically be modeled with a volume-averaged sum of concentrations in individual layers (Brigham and Smith 1965; Shook et al. 2009; Abbaszadeh-Dehghani and Brigham 1984). Although with some caveats, the 1D assumption provides a simple yet powerful model to analyze interwell tracer tests.

Many 1D analytic solutions for various combinations of boundary conditions are available in the literature (Lapidus and Amundson 1952; Danckwerts 1953; Pearson 1959; Lindstrom et al. 1967; Lindstrom 1969; Genuchten and Parker 1984; Cleary and Adrian 1973). Lapidus and Amundson (1952) presented analytic solutions for continuous concentration boundary conditions at the inlet (Dirichlet BC) and zero-gradient (Neumann) boundary conditions at the outlet in a semi-infinite domain. Danckwerts (1953) introduced the contribution of dispersion at the inlet boundary (Robin BC, or third type BC). This causes a concentration jump at the inlet of the domain relative to the injected concentration and ensures continuous flux at the inlet. Danckwerts (1953) used zero-gradient BC (or no dispersive flux) at the outlet (Neumann BC). Later, Pearson (1959) confirmed these boundary conditions via mathematical analysis.

The discussion regarding appropriate boundary condition choice has been ongoing for decades. Levenspiel noted that some authors propose “mathematically attractive, but physically absurd boundary conditions” (Levenspiel and Smith 1979). For highly dispersive formations, Danckwerts introduced the most appropriate boundary conditions for a packed column (Danckwerts 1953; Pearson 1959; Genuchten et al. 2013; Golz 2004; Kreft and Zuber 1978). Novakowski (1992) showed that, using the boundary conditions of Danckwerts, only the infinite series solution, obtained by Brenner, conserves mass. Van Genuchten et al. compiled several analytic solutions to the ADE for different boundary condition combinations (Genuchten and Parker 1984; Genuchten et al. 2013; Genuchten and Wierenga 1986; Parker 1984). In this study, we demonstrate that only the analytic solutions with Dirichlet BC at the inlet and semi-infinite domain, as well as Robin BC at the inlet and Neumann BC at the outlet (i.e., Danckwerts-type) are mass conservative across a broad range of dispersion coefficient values and, accordingly, are adopted here. The validity of these solutions at high dispersion coefficients is especially critical, as both laboratory and field tracer data from limestone formations, such as Arab D, exhibit high dispersivity.

In this study, we review current tracer flow models. We systematically assess published analytic solutions for conservative tracer flow and discuss their applicability limits based on the choice of boundary conditions. Next, we formulate a partitioning tracer flow model with non-equilibrium partitioning due to mass transfer limitations. We then compare remaining oil saturation estimates using equilibrium and non-equilibrium models, demonstrating potential errors and the applicability range of Cooke's equation. Additionally, we compare errors in remaining oil saturation estimates using traditional peak arrival times against the more rigorous mean arrival times. Finally, we apply our findings to analyze a published partitioning tracer dataset and compare our results with those of the original study (Sanni et al. 2016). In this study, we analyze dimensional concentration histories derived from solutions of non-dimensional ADEs. In contrast, Shook (2005) interprets field tracer tests using the residence time distribution as a function of time. Mathematical solutions of the ADE apply equally to both concentration histories and residence time distributions, provided the same average injection flow rate and injected mass are considered. The flow rate is nearly constant in the field case analyzed below. So, conversion between the two languages is straightforward.

2 Theory

Mass Conservation Equations for Tracer Transport

The one-dimensional macroscopic transport of any tracer traversing in the aqueous phase through a homogeneous porous medium in the presence of a stagnant oil phase is described by

$$\phi S_w \frac{\partial C_w}{\partial t} + u \frac{\partial C_w}{\partial x} - \phi S_w D_H \frac{\partial^2 C_w}{\partial x^2} = -r^{wo} \quad (1)$$

and

$$\phi S_o \frac{\partial C_o}{\partial t} = r^{wo} \quad (2)$$

where C_w and C_o are average tracer concentrations in the water and oil phases ($M L^{-3}$), respectively, u is the superficial (Darcy) velocity ($L T^{-1}$), D_H is the hydrodynamic dispersion coefficient in the longitudinal direction ($L^2 T^{-1}$), ϕ is the fluid-accessible porosity (-), S_w and S_o are saturations of water and oil (-), respectively, and r^{wo} denotes the rate of transfer of solute from the water phase and into the oil phase ($M L^{-3} T^{-1}$). The interstitial velocity, v , is given by $v = u/\phi S_w$. These equations assume constant porosity, uniform water and oil saturation throughout the domain, uniform Darcy velocity, and uniform and constant hydrodynamic dispersion coefficient along the longitudinal direction.

Conservative Tracer

An appropriate expression is needed for r^{wo} . For a conservative tracer, this term will be zero, meaning that only Eq. 1 with $r^{wo} = 0$ is needed. Thus,

$$\frac{\partial C_w}{\partial t} + v \frac{\partial C_w}{\partial x} - D_H \frac{\partial^2 C_w}{\partial x^2} = 0 \quad (3)$$

In dimensionless form, Eq. 3 becomes

$$\frac{\partial \tilde{C}_w}{\partial \tilde{t}} + \frac{\partial \tilde{C}_w}{\partial \tilde{x}} - \frac{1}{Pe_L} \frac{\partial^2 \tilde{C}_w}{\partial \tilde{x}^2} = 0 \tag{4}$$

where $Pe_L = vL/D_H$, $\tilde{x} = x/L$, $\tilde{t} = vt/L$, L is the characteristic length between inlet and outlet (injector and producer), and $\tilde{C}(x, t) = (C(x, t) - C_{init}) / (C_{inj} - C_{init})$, where subscripts “init” and “inj” denote initial and injected concentrations, respectively.

Partitioning Tracer—Equilibrium

For a partitioning tracer, two approaches are possible. If the rate of mass transfer from water to oil is fast relative to the advective flux, one may assume equilibrium partitioning; that is, the solute concentration in oil is an algebraic function of the solute concentration in water at any given location and time. Typically, a linear dependence is assumed as $C_o = KC_w$, where K is known as the partitioning coefficient (–). Summing Eqs. 1 and 2 and substituting KC_w for C_o , we obtain

$$R \frac{\partial C_w}{\partial t} + v \frac{\partial C_w}{\partial x} - D_H \frac{\partial^2 C_w}{\partial x^2} = 0 \tag{5}$$

where $R = 1 + KS_o / (1 - S_o)$ is the retardation factor. It is evident that we retrieve the mass conservation equation for a conservative solute by setting $R = 1$.

In dimensionless form, Eq. 5 becomes

$$R \frac{\partial \tilde{C}_w}{\partial \tilde{t}} + \frac{\partial \tilde{C}_w}{\partial \tilde{x}} - \frac{1}{Pe_L} \frac{\partial^2 \tilde{C}_w}{\partial \tilde{x}^2} = 0 \tag{6}$$

Partitioning Tracer—Non-equilibrium

In cases where the mass transfer rate is slow relative to the advective flux, the local equilibrium assumption is no longer valid. Two mass transfer processes arise in the system: mass transfer of partitioning tracer from the bulk aqueous phase to the concentration boundary layer near the brine–oil interface, and slow diffusion of the partitioning tracer from the oil–brine interface to the center of the oil blob. The latter process is typically limiting. As such, the mass transfer in the aqueous phase can be neglected and the mass conservation equation can be parameterized with the following linear kinetic process: $r^{wo} = \phi\alpha(KC_w - C_o)$. Then Eqs. 1 and 2 become

$$\phi S_w \frac{\partial C_w}{\partial t} + u \frac{\partial C_w}{\partial x} - \phi S_w D_H \frac{\partial^2 C_w}{\partial x^2} = -\phi\alpha(KC_w - C_o) \tag{7}$$

and

$$\phi S_o \frac{\partial C_o}{\partial t} = \phi\alpha(KC_w - C_o) \tag{8}$$

where $\alpha = a_v^i D_m^o / \delta$ is the diffusive mass-transfer rate coefficient for partitioning tracer oil phase diffusion (T^{-1}); a_v^i is the specific surface area of the oil–brine interface (L^{-1}); D_m^o is the partitioning tracer molecular diffusion coefficient in the oil ($L^2 T^{-1}$); and δ is the average transverse characteristic dimension of oil blobs (L). In the discussion pertaining to the partitioning tracer transport in the oil phase, the term mass transfer refers to the tracer transport by diffusion.

In dimensionless form, Eq. 7 for the mobile phase becomes

$$\frac{\partial \tilde{C}_w}{\partial t} + \frac{\partial \tilde{C}_w}{\partial x} - \frac{1}{Pe_L} \frac{\partial^2 \tilde{C}_w}{\partial x^2} = -\frac{Da_m}{S_w} (K\tilde{C}_w - \tilde{C}_o) \tag{9}$$

where $Da_m = a_v^i D_m^o L / \delta v$ is the mass transfer Damköhler number.

Then, Eq. 8 for the immobile oil phase becomes

$$\frac{\partial \tilde{C}_o}{\partial t} = \frac{Da_m}{S_o} (K\tilde{C}_w - \tilde{C}_o) \tag{10}$$

2.1 Boundary Conditions

The solution of these partial non-homogeneous differential equations requires two boundary conditions (BC) at the inlet and outlet for C_w , and two initial conditions for C_w and C_o . The initial conditions ($t = 0$) are $C_w(x, 0) = 0$ and $C_o(x, 0) = 0$. The choice of boundary conditions depends on the specific problem and physical conditions. Commonly used boundary conditions are summarized in Table 1.

The injected concentration for a pulse injection, $C_{inj}(t)$, is given by

$$C_{inj}(t) = \begin{cases} C_{inj}, & 0 < t \leq t_s \\ 0, & t > t_s \end{cases} \tag{11}$$

where t_s is the injected slug/pulse duration.

The analytic solution for a pulse injection of solute is given by

$$C(x, t) = \begin{cases} A(x, t), & 0 < t \leq t_s \\ A(x, t) - A(x, t - t_s), & t > t_s \end{cases} \tag{12}$$

where A is a superposition of complementary error functions, whose final form depends on the choice of boundary conditions. Analytic solutions for all the boundary conditions in Table 1 are presented in Appendix 1.

Table 1 Boundary conditions (BC) sets, their mathematical expressions for inlet and outlet, and references to authors who used them

BC set	BC inlet ($x = 0$)	BC outlet
DS (Lapidus and Amundson 1952)	Dirichlet $C(0, t) = C_{inj}(t)$	$\left. \frac{\partial C(x, t)}{\partial x} \right _{x=\infty} = 0$
DN (Cleary and Adrian 1973)	Dirichlet $C(0, t) = C_{inj}(t)$	$\left. \frac{\partial C(x, t)}{\partial x} \right _{x=L} = 0$
RS (Lindstrom et al. 1967; Lindstrom 1969)	Robin $C(0, t) - \frac{D_H}{v} \frac{\partial C(0, t)}{\partial x} = C_{inj}(t)$	$\left. \frac{\partial C(x, t)}{\partial x} \right _{x=\infty} = 0$
RN (Danckwerts 1953; Pearson 1959; Brenner 1962)	Robin $C(0, t) - \frac{D_H}{v} \frac{\partial C(0, t)}{\partial x} = C_{inj}(t)$	$\left. \frac{\partial C(x, t)}{\partial x} \right _{x=L} = 0$

The outlet BC at $x = \infty$ represents a semi-infinite domain, and at $x = L$ represents a finite domain (Neumann BC)

2.2 Mass Balance Analysis

For further analysis, it is useful to define the breakthrough time. The definition of breakthrough time varies across different fields. In hydrology, breakthrough time is defined as the appearance of the injected solute at $x = L$, using the mean residence time of an effluent (Danckwerts 1953; Shook 2005). In the geothermal field, breakthrough time refers to the arrival of the cold injection front at the production well. In the oil and gas industry, breakthrough time indicates the first appearance of an injected fluid at the outlet or producer (SLB Glossary: Breakthrough, <https://glossary.slb.com/en/terms/b/breakthrough>). The oil and gas industry does not typically use the mean residence time concept, although lately some authors have started using it (Shook 2005; Shook et al. 2009; Sanni et al. 2016). Unfortunately, the first appearance time provides minimal information for further analysis. Therefore, in the following, we use the mean residence time (MRT) as the breakthrough time.

Estimation of mean residence time depends on the type of injection (i.e., pulse or step). For continuous (step) injection, the breakthrough time is derived through mass balance (Danckwerts 1953; Levenspiel 1999; Yutkin et al. 2022). However, this definition for continuous injection is not required for our analysis, as we are focused on pulse injection schemes. For a pulse (slug) injection, the breakthrough time is determined using the method of moments, as the concentration-weighted arrival time normalized to the total injected mass minus one half the injected slug/pulse duration (Dwarakanath et al. 1999; Shook 2005; Levenspiel 1999).

$$t_b = \frac{\int_0^\infty C(x=L, t)t dt}{\int_0^\infty C(x=L, t) dt} - \frac{t_s}{2} \quad (13)$$

where t_b is the breakthrough or mean residence time, and t_s is the injected slug/pulse duration. It can be shown that Eq. 13 applies to dimensionless breakthrough curves as well. By definition, the dimensionless mean residence time or dimensionless breakthrough time of a conservative tracer is equals to unity. Note that, when the pulse duration is infinitesimally small, as in field-scale injection, the breakthrough time corresponds to the mean of the concentration distribution over time (breakthrough curve).

2.3 Remaining Oil Saturation

Cooke (1971) patented a method for determining fluid saturations in reservoirs, which involves the injection of tracers with different partitioning coefficients between an injector and a producer well, followed by measurement of the tracers' arrival times. Using mass balance and chromatography principles, and assuming an immobile oil phase, the remaining oil saturation in the probed volume is given by

$$S_o = \frac{t_b^p - t_b^c}{t_b^p + t_b^c(K - 1)} \quad (14)$$

where K is the partition coefficient, t_b^p is the arrival time of the partitioning tracer, and t_b^c is the arrival time of the conservative tracer. The term "arrival time" is used here intentionally, as in Cooke's patent, arrival time is determined by the location of the peak on the

concentration distribution curve (Cooke 1971). However, more rigorously, t_b^p and t_b^c should correspond to the mean residence times of partitioning and conservative tracers, respectively. The lack of distinction between peak and mean residence times can lead to errors in breakthrough data interpretation, as will be demonstrated below.

3 Methodology

The conservative tracer transport model used for the mass balance analysis (Eq. 4) was used in analytic form for the boundary conditions listed in Table 1, assuming zero initial conditions, $C_w(x, 0) = 0$. Further analyses utilized only Robin–Neumann boundary conditions, following validation that they were the most suitable BC for our highly dispersive systems (see Results section).

Next, the conservative tracer (Eq. 4) and equilibrium partitioning tracer transport (Eq. 6) models were used in the forms of both approximate and infinite series analytic solutions for Robin–Neumann boundary conditions (see Appendix 1).

The non-equilibrium partitioning tracer transport governing equations (Eqs. 9 and 10) were solved numerically in COMSOL. COMSOL verification is presented in Appendix 2.

Finally, the fitting of field IPTT data was based on a reverse-engineered process. Following Shook et al. (2009) for multilayer systems, the concentration breakthrough curve at the producer well represents the combined contributions of solutes from each layer and is given by

$$C(t) = \frac{\sum_{j=1}^N C_j(t)Q_j(t)}{\sum_{j=1}^N Q_j(t)}; \quad j = 1, 2, \dots, N \quad (15)$$

where Q_j is the flow rate of layer j , $C_j(t)$ is the concentration history of layer j , and N is the number of layers. First, we fitted the conservative tracer data with the analytic solution under RN boundary conditions. The best-fitting model was obtained by solving an optimization problem, where breakthrough time and Péclet number were the fitting parameters. Breakthrough time (MRT) cannot be determined from incomplete highly skewed concentration histories. But rather, MRT has to be obtained by fitting a physically appropriate model to the incomplete data.

Data used as input in the model are the interwell distance (610 m), and the average injection rate (8000 BPD), derived from the $E(t)$ and $C(t)$ relationship, and the data reported in Sanni et al. (2015). The model has two dimensionless parameters, which are the Péclet number and the mean residence time (MRT). In dimensional units, these correspond to fitting the interstitial velocity and hydrodynamic dispersion coefficient. The analytic solution was computed in dimensionless units with the assumed Péclet number and then scaled to dimensional units using the assumed breakthrough time. This process was repeated across a range of Péclet numbers and breakthrough times, and the solution with the least error was chosen.

Then, reference Péclet number and breakthrough time from the best-fitting conservative tracer model were used in both equilibrium and non-equilibrium partitioning tracer models. Fitting the partitioning models to the partitioning data involved another optimization problem, with oil saturation and Damköhler number as fitting parameters. For the equilibrium model, only oil saturation was a fitting parameter. The partitioning tracer models were solved numerically in COMSOL in dimensionless units, then scaled to dimensional units

using the breakthrough time from the conservative tracer fit. This process was repeated for oil saturations from 0.1 to 0.3, in linearly spaced sampling intervals, and for Damköhler numbers (non-equilibrium partitioning) between 1×10^{-4} and 1×10^4 , in logarithmically spaced sampling intervals. The numerical solution with the least error (L_2 -norm) was selected as the best-fit.

4 Results

4.1 Mass Balance Analysis

We begin validation of the analytic solutions for Eq. 4 by calculating the mean residence time (MRT) using the method of moments, as outlined in the Theory section.

For a conservative tracer with an infinitesimally small injection volume, the dimensionless MRT should be unity (i.e., one pore volume). If the dimensionless MRT deviates from unity for a given solution, it indicates issues with mass conservation. Using this criterion, we assess the validity range of the analytic solutions of the ADE (Eq. 4) under the various boundary conditions presented in Table 1.

Figure 1a presents conservative tracer concentration breakthrough curves obtained from the analytic solutions of Eq. 4 for all four sets of boundary conditions in Table 1, shown on a dimensionless scale with a Péclet number equal to two. Each concentration breakthrough curve exhibits a distinct shape. The vertical lines indicate the dimensionless breakthrough times (\tilde{t}_b) of each curve. Although the graph is truncated at three pore volumes, the analysis was conducted over the entire dataset, extending up to 15 pore volumes (further extension of the calculation domain did not affect the results).

When the calculated MRT deviates from unity, mass is not conserved. Thus, the mass balance analysis shows that at $Pe_L = 2$, two analytic solutions Robin SemiInf (RS) and Dirichlet Neumann (DN)-do not conserve mass, while two solutions—Dirichlet SemiInf

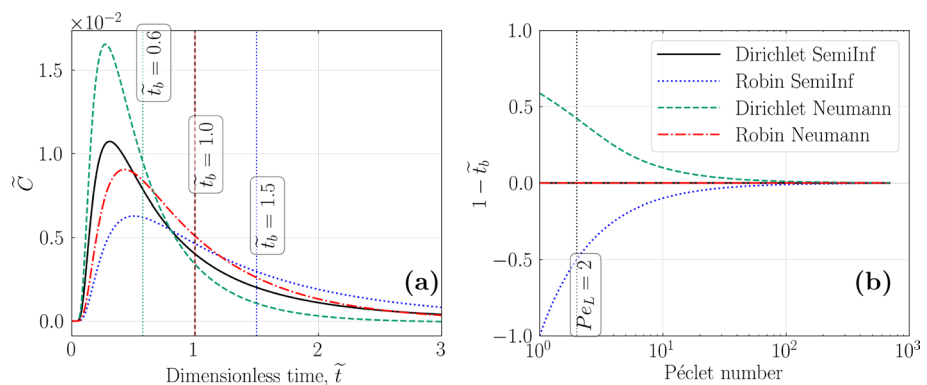


Fig. 1 **a** Analytic concentration histories for conservative tracer pulse at boundary conditions presented in Table 1. The vertical lines with annotations show the calculated breakthrough times (\tilde{t}_b) using Eq. 13. $Pe_L = 2$. $\tilde{x} = 1$. $\tilde{t}_s = 0.01$. **b** Absolute mean residence time residuals for conservative tracer at different Péclet numbers. RN plots for $Pe_L < 3$ were obtained with Brenner infinite series analytic solution (Brenner 1962). For $Pe_L \geq 3$ we use the RN approximated analytic solution (see Appendix 1). The black vertical dashed line corresponds to the example in the left graph ($Pe_L = 2$)

(DS) and Robin–Neumann (RN)—do conserve mass. These findings align with the results obtained by Van Genuchten and Wierenga, who compared the “holdup” of different solutions with the theoretical retardation factor.

Figure 1b examines the mass conservation error in the four analytic solutions across a broad range of longitudinal Péclet numbers, from 1 to 500. We plot the conservative tracer MRT (i.e., must be equal unity) residuals vs. a range of Péclet numbers. At longitudinal Péclet numbers above 100, all four analytic solutions perform very well in terms of mass conservation. However, below $Pe_L = 100$, both RS and DN solutions fail to conserve mass, and the mass conservation error increases as the Péclet number decreases.

The analytic solutions for DS and RN boundary conditions (see Appendix 1) maintain mass conservation over a wide range of Péclet numbers down to $Pe_L = 3$. Below this threshold, both solutions exhibit a minor mass conservation issue. Notably, Brenner’s (1962) infinite series solution conserves mass perfectly even at $Pe_L < 3$. Our findings on mass conservation error are consistent with the conclusions drawn by Novakowski (1992).

Thus, for a highly dispersive formation, careful selection of boundary conditions is essential. We demonstrate that only the analytic solutions with Dirichlet SemiInf and Robin–Neumann BC are mass conservative across a broad range of Péclet numbers. The validity of these solutions at low Péclet numbers is especially critical, as both laboratory and field tracer data from limestone formations, such as Arab D, exhibit high dispersivity and, consequently, low Péclet numbers (Yutkin et al. 2022). Using non-mass-conservative solutions to describe tracer flow in such rock leads to a significant misrepresentation of the rock properties.

4.2 Estimation of Remaining Oil Saturation

The transport of a conservative tracer is governed by Eq. 3 (or Eq. 4 in dimensionless form), whereas the transport of an equilibrium partitioning tracer is governed by Eq. 5 (or Eq. 6 in dimensionless form). Using Eq. 6, the remaining oil saturation can be readily calculated from the breakthrough times of both tracers and the partitioning coefficient measured in the laboratory. This calculation follows the well-known Cooke’s equation (Eq. 14).

Figure 2a illustrates the successful application of Cooke’s equation for estimating remaining oil in a system where the partitioning tracer attains equilibrium conditions. Two tracers are injected simultaneously into a model system containing 20% stagnant remaining oil. The conservative tracer arrives at 1 pore volume (PV), as indicated by the dimensionless breakthrough time of unity. The partitioning tracer is delayed according to the linear adsorption isotherm with $K = 2$ (corresponding to $R = 1.5$) and thus arrives at a dimensionless breakthrough time of 1.5. These breakthrough times are then input into Eq. 14, yielding a remaining oil saturation of 0.2, which perfectly matches the reference value.

In the oil and gas literature, tracer breakthrough times are often replaced with tracer peak times. Tracer peaks are indeed much easier to identify, as they require no computational analysis and can simply be assigned by eye, assuming they are not missed during measurements. During an IPTT, determining the MRT may take several years of well flooding because it requires capturing the entire breakthrough curve, whereas peaks often appear within a much shorter time frame, facilitating quicker decision-making. However, using peak time instead of MRT to estimate tracer breakthrough time is valid only when breakthrough curves are symmetric, which is typically not the case. For skewed

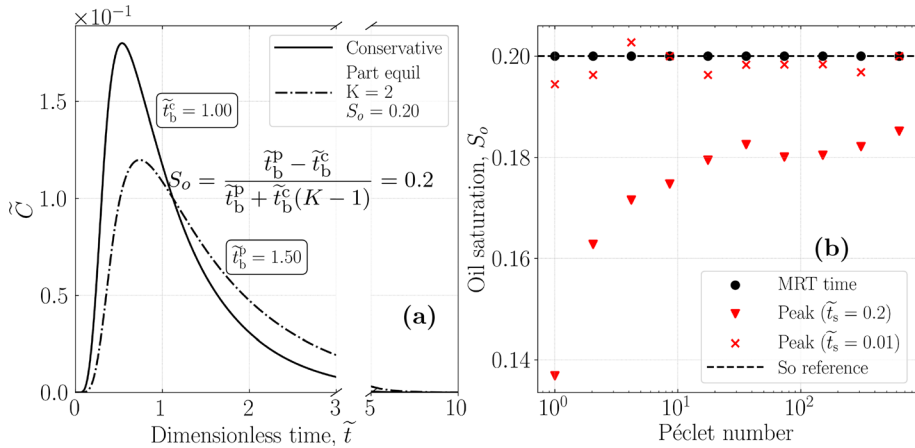


Fig. 2 **a** Dimensionless concentration histories of conservative (solid line) and partitioning (dot-dashed line) tracers at equilibrium. $\tilde{x} = 1$. $Pe = 2$. $\tilde{t}_s = 0.2$. For partitioning tracer, $S_o = 0.2$ and $K = 2$ ($R = 1.5$). \tilde{t}_b^c and \tilde{t}_b^p are the calculated breakthrough times of the conservative and partitioning tracers, respectively. **b** Remaining oil saturation calculated using Cooke’s equation at various Péclet numbers, for conservative and equilibrium partitioning tracers. Black filled circles are calculated using mean residence time. Red filled triangles and crosses are calculated using the peak (mode) of the concentration distributions for $\tilde{t}_s = 0.2$ and $\tilde{t}_s = 0.01$, respectively. $K = 2$, reference oil saturation, $S_o = 0.2$, and $Pe_L = 2$

breakthrough curves, a mass balance analysis (see Theory section) must be conducted to determine the tracer’s breakthrough time accurately.

Figure 2b compares the deviation of remaining oil saturation estimates obtained using peak and breakthrough times across different Péclet numbers and injected tracer pulse volumes. The reference oil saturation of 0.2 is consistently obtained using the mean residence time (solid black circles), regardless of pulse injection size. However, using peak time for large tracer pulses—typical of laboratory experimental setups (for example, $\tilde{t}_s = 0.2$)—leads to substantial underestimation of remaining oil (red triangles). Conversely, using very short but concentrated tracer pulses, which is typical in field tracer tests, introduces only a minor error in the estimated oil saturation (red crosses).

We can therefore conclude that using peak time for very short tracer pulses ($\tilde{t}_s \leq 0.01$) may be acceptable for estimating remaining oil, provided that equilibrium is reached. Despite this close agreement, Cooke’s equation must be applied with caution if the partitioning equilibrium assumption does not hold. We address this case below.

Non-equilibrium in tracer partitioning arises from the slow diffusion of large tracer molecules toward the center of oil blobs or patches, or when the advection rate exceeds the mass transfer rate, preventing equilibrium from being reached. Non-equilibrium in partitioning tracers is described by Eqs. 7 and 8 (or in dimensionless form, Eqs. 9 and 10). Therefore, Cooke’s equation is valid only under certain conditions where non-equilibrium effects are limited.

Three types of behavior for Eqs. 7 and 8 can be deduced by examining the following extreme cases. First, when the mass transfer rate is much greater than the flow rate (i.e., $Da_m \gg 1$), the equilibrium concentration of the partitioning tracer in the oil phase is attained, making this process equivalent to the equilibrium case described above. Second, when the mass transfer rate is much slower than the flow rate ($Da_m \ll 1$), no partitioning tracer enters the oil phase, rendering the scenario equivalent to conservative tracer

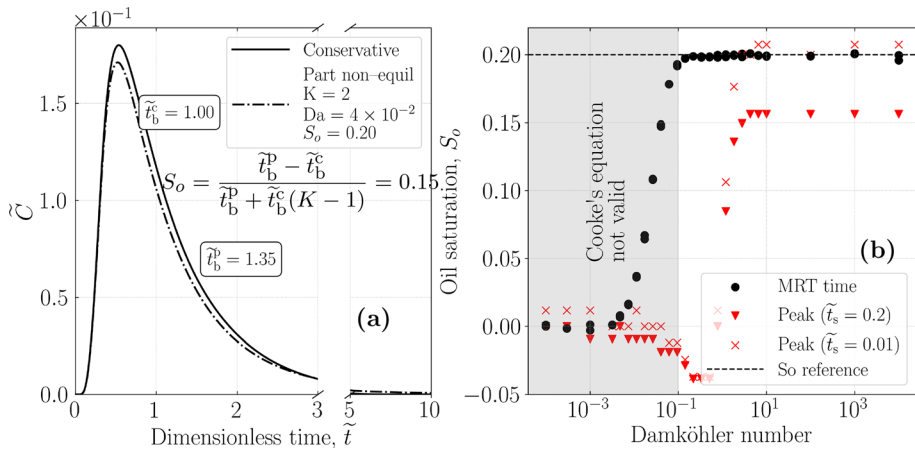


Fig. 3 **a** Dimensionless concentration histories of conservative (solid line) and partitioning (dot-dashed line) tracers at non-equilibrium conditions. $\tilde{x} = 1$. $Pe_L = 2$. $\tilde{\tau}_s = 0.2$. For the partitioning tracer, $S_o = 0.2$ and $K = 2$ ($R = 1.5$). \tilde{t}_b^c and \tilde{t}_b^p are the calculated breakthrough times of the conservative and partitioning tracer, respectively. **b** Remaining oil saturation calculated with Cooke’s equation under different Damköhler numbers using the non-equilibrium partitioning tracer model. Black filled circles are calculated using mean residence time. Red triangles and crosses are calculated using the peak (mode) of the concentration distributions for $\tilde{\tau}_s = 0.2$ and $\tilde{\tau}_s = 0.01$, respectively. $K = 2$, reference oil saturation, $S_o = 0.2$, and $Pe_L = 2$

flow. Finally, when the mass transfer and flow rates are approximately equal ($Da_m \sim 1$), an intermediate case occurs, requiring a numerical solution to determine the remaining oil saturation.

Figure 3a demonstrates the failure of Cooke’s equation for estimating remaining oil in a non-equilibrium system. Two tracers are injected simultaneously into a model system containing 20% stagnant remaining oil. The conservative tracer arrives with a mean residence time equal to unity. The maximum delay of the partitioning tracer corresponds to the linear adsorption isotherm with $K = 2$. However, due to non-equilibrium partitioning, the mean residence time of the partitioning tracer is 1.35, which is sooner than in the equilibrium case ($R = 1.5$). Substituting the obtained mean residence times of the conservative and partitioning tracers into Eq. 14 yields a remaining oil saturation of 0.15, which does not match the reference value of 0.2.

Figure 3b graphically shows the deviation of the remaining oil saturation from the reference value of 0.2, obtained using peak and breakthrough times at $Pe_L = 2$ across a range of non-equilibrium conditions characterized by the Da_m number. Using mean residence time allows for an accurate estimation of remaining oil at $Da_m > 0.1$ (solid black circles) when applying Cooke’s equation. If minor deviation is acceptable, this limit can be slightly reduced. Conversely, using peak times to estimate remaining oil saturation is generally unjustified. For large tracer pulses, such as those typical in the laboratory, there is significant underestimation of remaining oil even at high Da_m values ($Da_m > 10$), as indicated by the red triangles in Fig. 3b. Short tracer pulses do not improve accuracy; for $Da_m > 10$ (approaching equilibrium conditions), using peak time leads to an overestimation of remaining oil, which is a more unfavorable error from a financial perspective.

These results are presented for $Pe_L = 2$. At high Péclet numbers, the tracer breakthrough profiles become symmetric, and the difference between the peak and mean of the concentration distribution for the conservative tracer vanishes. For partitioning tracers

under non-equilibrium conditions, however, truly symmetric peaks cannot be achieved due to delayed release times from the oil phase. We present the results for $Pe_L = 100$ in Appendix 3. At high Péclet numbers, the MRT (Eq. 13) becomes interchangeable with $t_b = t_{\text{peak}} - t_s/2$, providing an accurate remaining oil saturation estimate using Cooke's equation. In other words, instead of using peak time directly in Cooke's equation, it is preferable to use t_b calculated from the peak time. Note that this approach is only valid at high Péclet numbers, where the analytic solutions are symmetric.

The values of Da_m can be estimated if the petrophysical properties of the formation, along with oil physical properties and flow velocity, are known. Such estimates can guide the selection of an appropriate model to interpret experimental or field data. For example, Table 2 presents Da_m values bracket for a wide range of properties (see Appendix 4). Although Da_m may vary widely, the range can be significantly narrowed when specific formation and oil properties are known.

4.3 Field Application

In this section, we apply our physics-based approach to published interwell tracer data to estimate the remaining oil saturation (Sanni et al. 2015, 2016, 2017).

We employ our approach to analyze results from an interwell partitioning tracer test conducted after a successful waterflooding of a Jurassic-age carbonate reservoir (Sanni et al. 2015, 2016, 2017). Consequently, remaining oil saturation conditions were expected. Geological characterization indicates that the reservoir is a dual-layer carbonate system; one layer consists of diagenetic dolomites (referred to below as the first layer), which is believed to facilitate fast breakthrough (Sanni et al. 2017). The configuration includes an injector and a producer well, separated by approximately 610 m. The field test involved injecting one conservative tracer, WT-60, and three partitioning tracers, WTP-2 ($K = 2.1$), WTP-3 ($K = 2.1$), and WTP-4 ($K = 4$). Reported injected concentrations were a 28.6 kg/m³ solution for the conservative tracer and 1000 kg/m³ (most probably as 100% active material) for the partitioning tracers. According to Sanni et al. (2016), "the tracers were added "on-the-fly" during normal operation of the water injection wells and were thereby diluted to low ppm concentrations in the injection water immediately". The actual injected concentration after dilution is unknown. Upon closer examination, the published datasets appear to originate from different experiments. We use the data presented by Sanni et al. (2016).

The original approach in Sanni et al. (2016) employs an analytic solution proposed by Viig et al. (2013). The fitting parameters for this type curve included total mass injected, dispersion coefficient, and pulse time. Their estimation of remaining oil saturation was based on independent curve fittings of the conservative and partitioning tracer breakthrough curves using Viig et al.'s type curve. While this is a viable approach, it disregards the continuity of physical properties between conservative and partitioning tracer flows.

In contrast, our approach fits coupled conservative and partitioning tracer equations, consistent with the physical representation of the reservoir, resulting in improved fit quality.

Moreover, the analytic solution used in the original study applied non-mass-conservative boundary conditions, meaning it does not conserve mass at the longitudinal Péclet numbers observed in the reservoir. In our approach, we use a validated analytic solution for conservative tracer flow and apply the same boundary conditions for all further analyses.

The original study uses peak times and MRT as input to Cooke's equation for estimating remaining oil. However, the final predictions of remaining oil based on peak times were considered more accurate, as those did not depend on data extrapolation. In our approach, we base the remaining oil interpretation on tracer mean residence times. Where necessary, we solve the partitioning tracer flow numerically, as Cooke's equation is not applicable for remaining oil estimation under non-equilibrium partitioning conditions, which are present in this reservoir.

Despite these shortcomings, we assume the reported average remaining oil saturation of 0.2 in the original study is accurate, as it was cross-validated using other reservoir characterization methods. To the best of our knowledge, no records exist in the literature of this analysis or similar approaches being applied to field-scale interwell tracer data.

Figure 4 presents conservative tracer concentration histories, $C(t)$ (solid black circles), converted from digitized residence time distributions, $E(t)$, (Sanni et al. 2016) using the mass injected and the average injection rate obtained from Sanni et al. (2015). Conservative tracer concentration breakthrough data (filled black circles) is fitted with the Robin–Neumann analytic solution (black line). Data used as input to the model are the interwell distance (610 m) and average injection rate calculated from Sanni et al. (2015). The fit of the analytic solution optimizes Péclet number and mean residence time. In dimensional units, the fit parameters are the interstitial velocity and hydrodynamic dispersion coefficient. The tracer concentration data shows two peaks at approximately 240 and 830 days, with mean residence times of 380 and 870 days, respectively. Following Shook et al. (2009) for multilayer systems, the concentration breakthrough curve at the producer well represents the combined contributions of solutes from each layer and is given by Eq. 15.

The solid black line in Fig. 4 represents the best fit for the tracer concentration breakthrough data. The volumetric flow distribution is 0.85 for the first layer and 0.15 for the second layer. The volumetric flow distribution follows an optimization problem constrained

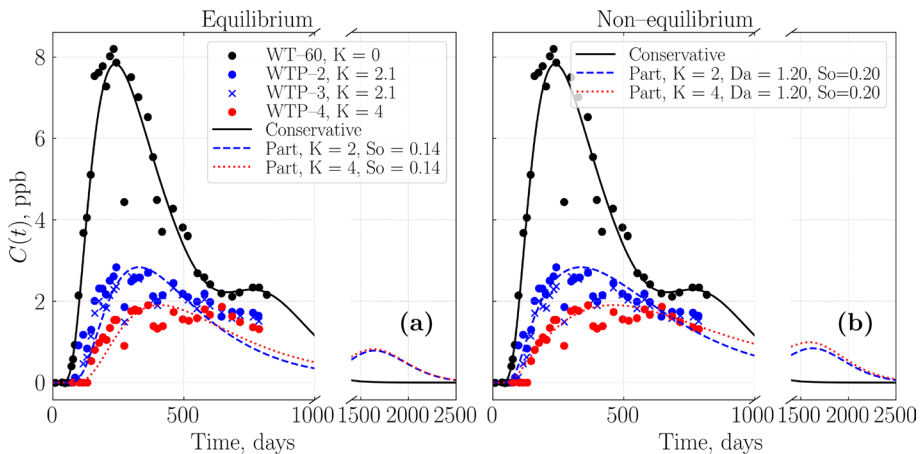


Fig. 4 Dimensional field concentration histories modeled with **a** equilibrium partitioning conditions and **b** non-equilibrium partitioning conditions for the first layer with $Da_m = 1.2$ and assuming that the second layer has finite remaining oil. The black filled circles represent the conservative tracer WT-60; blue filled circles and crosses represent the partitioning tracers WTP-2 and WTP-3, both with $K = 2.1$; red filled circles represent the partitioning tracer WTP-4 with $K = 4$. The blue dashed and red dotted lines correspond to partitioning tracer models for $K = 2$ and $K = 4$, respectively. The remaining oil saturation in the second layer is arbitrarily taken as 0.2 and modeled assuming equilibrium partitioning

by the relationship between the injected pulse time of the first layer ($t_{s,1}$) and the injected pulse time of the second layer ($t_{s,2}$). $t_{s,1} = ft_{s,2}$ are related by a factor, f , that depends on the ratio of velocity between the layers ($f = v_1/v_2$).

Based on the conservative tracer fit results, we can conclude that the mean interstitial fluid velocity in the second layer ($v = 0.7$ m/day) is approximately 2.3 times slower than in the first layer ($v = 1.6$ m/day). The hydrodynamic dispersion in the first layer is 2.27×10^{-3} m²/s ($Pe_L = 5$), while it is 8.25×10^{-5} m²/s in the second layer ($Pe_L = 60$). Similar or higher values of dispersion coefficients have been found in the literature (Parker 1984; Yutkin et al. 2022). Finally, the total recovered mass of the conservative tracer is 46%, suggesting that the partitioning tracer models should yield a comparable recovery.

Using the mean fluid velocity and hydrodynamic dispersion parameters for the two layers, we apply both equilibrium and non-equilibrium partitioning models to estimate remaining oil in this formation.

Figure 4a presents field data and fitted concentration breakthrough curves for the conservative tracer and two partitioning tracers (blue dashed line for $K = 2$ and red dotted line for $K = 4$), considering remaining oil in both layers and fast tracer partitioning in both layers (i.e., equilibrium conditions). The transport of partitioning tracers in both layers is described by Eq. 5.

In this scenario, the partitioning tracer model generates two distinct peaks, at approximately 400 and 1600 days. The first peak indicates the remaining oil saturation in the first layer, while the second peak reflects the remaining oil saturation in the second layer. However, the available data only spans around 800 days, so the saturation in the second layer cannot be inferred directly. For demonstration purposes, we have assigned a saturation value of 0.2 in the second layer.

The best-fit equilibrium model for the first peak appears slightly after the data for early time, suggesting shorter tracer retention in the field. However, the data's deviation from the model at later times indicates longer tracer retention in the field. This behavior is characteristic of non-equilibrium tracer partitioning, where the tracer arrives at the producer well quickly, followed by a prolonged spread. Therefore, we conclude that the partitioning tracer is not in an equilibrium state. The remaining oil in the first layer, estimated using Eq. 14, is 0.14.

The total recovered tracer amount comprises contributions from both the first and second layers. Since no data are available for the second layer, it is impossible to estimate its contribution accurately. The second layer may uptake $\sim 41\%$ of the recoverable partitioning tracer in the equilibrium case, and $\sim 26\%$ in the non-equilibrium case, potentially indicating a substantial amount of remaining oil, whether recoverable or not.

Figure 4b presents field data with fitted concentration breakthrough curves for the conservative tracer and two partitioning tracers (blue dashed line for $K = 2$ and red dotted line for $K = 4$), assuming non-equilibrium conditions ($Da_m = 1.2$) in the first layer and equilibrium partitioning with finite remaining oil in the second layer. Consequently, the transport of the partitioning tracer in the first layer is described by Eqs. 7 and 8, while in the second layer it is described by Eq. 5.

The Péclet number is fixed, and only two fitting parameters are required to fit the models: remaining oil saturation and the Damköhler number in the first layer. As before, the saturation in the second layer is arbitrarily set to 0.2 for demonstration purposes. The resulting Damköhler value is near unity, indicating non-equilibrium conditions.

In this scenario, the partitioning tracer elutes as two peaks, one from each layer. As expected, the initial elution of the peaks occurs sooner than under equilibrium conditions, followed by a longer spread. These combined features result in notably better fits

to the experimental data. Similar to the equilibrium case above, effects from the second layer are not yet observed and would only begin to emerge around 1500 days.

Finally, the estimation of remaining oil saturation in the first layer (obtained by directly solving the governing ODE) yields a value of 0.2, consistent with the cross-validated value reported by the authors of the original study. However, the remaining oil saturation in the second layer is not captured and cannot be estimated. According to observations presented in Sanni et al. (2017), the second layer is thicker than the first layer. The combination of a large pore volume and higher than anticipated oil saturation in the second layer leads to a longer delay in arrival of the second peak.

5 Discussion

As we showed above, the remaining oil saturation in the first layer is close to 0.2. Unfortunately, due to the lack of critical data for this field case, no definitive or quantitative conclusions can be made regarding the remaining oil saturation in the second layer. Appendix 5 presents a simple scenario using the 4% oil cut reported in the original IPTT study. We show that the effect of the oil cut is negligible.

To improve the analysis of interwell partitioning tracer tests, we suggest collecting the following data: (1) flow rate history from spinner surveys at the injector and producer wells, which would help accurately determine the fractional flow into multiple layers, if present; (2) information on wellbore mixing in the injector and producer wells, and/or tracer concentrations measured in the injection wellbore at the injection interval. Additionally, longer data collection even at wider time intervals will allow on to estimate remaining oil in lower permeability reservoir sections.

Since interwell partitioning tracer tests provide average property estimates over large areas, it is essential to correlate the extracted information with any additional data available in the study area. If observation wells exist, they could provide earlier estimates of flow properties, particularly partitioning tracer data, which generally takes longer to arrive.

6 Conclusions

In this study, we developed a 1D partitioning tracer transport model that has not been previously published. Alongside our new model, we examined the applicability range of other published 1D tracer flow models for both conservative and partitioning tracers. To ensure mass conservation across a wide range of flow conditions for history matching, in analytic and numerical solutions for tracer flow (i.e., both conservative and partitioning), one must use Robin–Neumann boundary conditions, especially at low Péclet numbers ($Pe_L \lesssim 20$), which characterize many carbonate pore systems.

We demonstrate that using tracer peaks to estimate remaining oil is not always appropriate. Use of peak time for very short tracer pulses ($\tilde{\tau}_s \leq 0.1$) may be acceptable for estimating remaining oil, provided that equilibrium is reached quickly ($Da_m \gg 1$), otherwise not so. Mean Residence Time (MRT) is the accurate way to describe the breakthrough of tracers. MRT provides an accurate estimate of remaining oil saturation using Cooke's equation, but only provided that $Da_m > 0.1$. Additionally, we highlighted the consequences of using an incorrect model for partitioning tracers. Assuming an equilibrium model by

default can lead to either underestimation or overestimation of remaining oil saturation when tracer partitioning into the oil phase is slow, and the partitioning process does not reach equilibrium before tracer breakthrough, i.e., in systems with $Da_m \lesssim 1$. Moreover, Cooke's equation is no longer valid below $Da_m \leq 0.1$. The overestimation of remaining oil is a financially unfavorable outcome in an interwell partitioning test.

Finally, we analyzed published interwell partitioning tracer data, applying the insights gained from our 1D non-equilibrium study. We found that the field under investigation consisted of at least two layers that permitted the transport of both conservative and partitioning tracers. The first layer contained oil and facilitated fast tracer transport, making it necessary to apply our non-equilibrium partitioning model. Based on mass balance, we concluded that the second layer also contained oil. However, due to the lack of long-term field data, it was not possible to make quantitative conclusions regarding the amount of oil in the second layer. Our final estimates of remaining oil in the first layer are consistent with those made by the original authors' study. Therefore, our physics-based approach provides a robust foundation for understanding partitioning tracer test results in 1D, which can be extended to interpret more complex 3D models. Based on our analysis, we provide recommendations on additional data that could enhance the understanding of this and future interwell tracer tests.

Appendix 1: Analytic Solutions

Below are boundary condition-dependent analytic expressions for the term A (see Eq. 12). Full form of analytic solutions for both pulse and step injection can be composed using Eq. 12 of the main text. These solutions can be applied to a conservative tracer ($R = 1$), or a partitioning tracer under equilibrium conditions ($R > 1$). For an equilibrium partitioning tracer, divide the time variable t (or \tilde{t}) by R .

Inlet BC: Dirichlet; Domain: semi-infinite (DS) The analytic solution to these boundary conditions is given by Genuchten et al. (2013).

$$A(x, t) = \frac{1}{2} \operatorname{erfc} \left[\frac{x - ut}{\sqrt{4D_H t}} \right] + \frac{1}{2} \exp \left(\frac{ux}{D_H} \right) \operatorname{erfc} \left[\frac{x + ut}{\sqrt{4D_H t}} \right] \quad (16)$$

In dimensionless form,

$$A(\tilde{x}, \tilde{t}) = \frac{1}{2} \left\{ \operatorname{erfc} \left[\frac{\sqrt{\operatorname{Pe}} (\tilde{x} - \tilde{t})}{2 \sqrt{\tilde{t}}} \right] + \exp(\operatorname{Pe} \tilde{x}) \operatorname{erfc} \left[\frac{\sqrt{\operatorname{Pe}} (\tilde{x} + \tilde{t})}{2 \sqrt{\tilde{t}}} \right] \right\} \quad (17)$$

Inlet BC: Dirichlet; Outlet BC: Neumann (DN)

The analytic solution to these boundary conditions is given by Genuchten et al. (2013).

$$\begin{aligned}
 A(x, t) = & \frac{1}{2} \operatorname{erfc} \left[\frac{x - ut}{\sqrt{4D_H t}} \right] + \frac{1}{2} \exp \left(\frac{ux}{D_H} \right) \operatorname{erfc} \left[\frac{x + ut}{\sqrt{4D_H t}} \right] \\
 & + \frac{1}{2} \left(2 + \frac{u(2L - x)}{D_H} + \frac{u^2 t}{D_H} \right) \exp \left(\frac{uL}{D_H} \right) \operatorname{erfc} \left[\frac{(2L - x + ut)}{\sqrt{4D_H t}} \right] \\
 & - \sqrt{\frac{u^2 t}{\pi D_H}} \exp \left(\frac{uL}{D_H} - \frac{(2L - x + ut)^2}{4D_H t} \right)
 \end{aligned} \tag{18}$$

In dimensionless form,

$$\begin{aligned}
 A(\tilde{x}, \tilde{t}) = & \frac{1}{2} \operatorname{erfc} \left[\frac{\sqrt{\operatorname{Pe}} (\tilde{x} - \tilde{t})}{2 \sqrt{\tilde{t}}} \right] + \frac{1}{2} \exp (\operatorname{Pe} \tilde{x}) \operatorname{erfc} \left[\frac{\sqrt{\operatorname{Pe}} (\tilde{x} + \tilde{t})}{2 \sqrt{\tilde{t}}} \right] \\
 & + \frac{1}{2} (2 + \operatorname{Pe}(2 - \tilde{x} + \tilde{t})) \exp (\operatorname{Pe}) \operatorname{erfc} \left[\frac{\sqrt{\operatorname{Pe}} (2 - \tilde{x} + \tilde{t})}{2 \sqrt{\tilde{t}}} \right] \\
 & - \sqrt{\frac{\operatorname{Pe} \tilde{t}}{\pi}} \exp \left(\operatorname{Pe} - \frac{\operatorname{Pe}}{4 \tilde{t}} (2 - \tilde{x} + \tilde{t})^2 \right)
 \end{aligned} \tag{19}$$

Inlet BC: Robin; Domain: semi-infinite (RS)

The analytic solution to these boundary conditions is given by Genuchten et al. (2013).

$$\begin{aligned}
 A(x, t) = & \frac{1}{2} \operatorname{erfc} \left[\frac{x - ut}{\sqrt{4D_H t}} \right] + \sqrt{\frac{u^2 t}{\pi D_H}} \exp \left(-\frac{(x - ut)^2}{4D_H t} \right) \\
 & - \frac{1}{2} \left(1 + \frac{ux}{D_H} + \frac{u^2 t}{D_H} \right) \exp \left(\frac{ux}{D_H} \right) \operatorname{erfc} \left[\frac{x + ut}{\sqrt{4D_H t}} \right]
 \end{aligned} \tag{20}$$

In dimensionless form,

$$\begin{aligned}
 A(\tilde{x}, \tilde{t}) = & \frac{1}{2} \operatorname{erfc} \left[\frac{\sqrt{\operatorname{Pe}} (\tilde{x} - \tilde{t})}{2 \sqrt{\tilde{t}}} \right] + \sqrt{\frac{\operatorname{Pe} \tilde{t}}{\pi}} \exp \left(-\frac{\operatorname{Pe} (\tilde{x} - \tilde{t})^2}{4 \tilde{t}} \right) \\
 & - \frac{1}{2} (1 + \operatorname{Pe} \tilde{x} + \operatorname{Pe} \tilde{t}) \exp (\operatorname{Pe} \tilde{x}) \operatorname{erfc} \left[\frac{\sqrt{\operatorname{Pe}} (\tilde{x} + \tilde{t})}{2 \sqrt{\tilde{t}}} \right]
 \end{aligned} \tag{21}$$

Inlet BC: Robin; Outlet BC: Neumann (RN)

Two solutions exist for these BCs: one infinite series, which works well for high dispersivity (low Péclet numbers) (Brenner 1962), and one approximated solution which performs well after a Péclet threshold (Danckwerts 1953; Genuchten and Parker 1984; Genuchten et al. 2013).

$$A(\bar{x}, \bar{t}) = 2 \exp\left(\frac{Pe}{4}(2\bar{x} - \bar{t})\right) \sum_{k=1}^{\infty} \frac{\frac{Pe}{4} \lambda_k \exp\left(-\frac{4\lambda_k^2 \bar{t}}{Pe}\right)}{\left(\lambda_k^2 + \frac{Pe^2}{16} + \frac{Pe}{4}\right)\left(\lambda_k^2 + \frac{Pe^2}{16}\right)} \left[\lambda_k \cos(2\lambda_k \bar{x}) + \frac{Pe}{4} \sin(2\lambda_k \bar{x})\right] \tag{22}$$

where $\lambda_k (k = 1, 2, 3)$ are the positive roots, taken in order of increasing magnitude of the transcendental equation

$$\tan 2\lambda = \frac{\lambda \frac{Pe}{2}}{\lambda^2 - \frac{Pe^2}{16}} \tag{23}$$

from which the trivial root $\lambda_0 = 0$ is to be excluded. The numerical values of these roots at various Péclet numbers can be obtained from the tabulation of Carslaw and Jaeger (1959) by writing

$$\lambda_{2n-1} = \beta_n; \lambda_{2n} = \gamma_n \tag{24}$$

for $n = 1, 2, 3, \dots$, where the β_n and γ_n are the positive roots, taken in order, of the transcendental equations

$$\beta \tan \beta - \frac{Pe}{4} = 0 \tag{25}$$

and

$$\gamma \cot \gamma + \frac{Pe}{4} = 0, \tag{26}$$

respectively.

The approximated solution is

$$A(x, t) = \frac{1}{2} \operatorname{erfc}\left[\frac{x - ut}{\sqrt{4D_H t}}\right] + \sqrt{\frac{u^2 t}{\pi D_H}} \exp\left(-\frac{(x - ut)^2}{4D_H t}\right) - \frac{1}{2} \left(1 + \frac{ux}{D_H} + \frac{u^2 t}{D_H}\right) \exp\left(\frac{ux}{D_H}\right) \operatorname{erfc}\left[\frac{x + ut}{\sqrt{4D_H t}}\right] + \sqrt{\frac{4u^2 t}{\pi D_H}} \left[1 + \frac{u}{4D_H}(2L - x + ut)\right] \exp\left(\frac{uL}{D_H} - \frac{(2L - x + ut)^2}{4D_H t}\right) - \frac{u}{D_H} \left\{ \left[2L - x + \frac{3ut}{2} + \frac{u}{4D_H}(2L - x + ut)^2\right] \exp\left(\frac{uL}{D_H}\right) \operatorname{erfc}\left[\frac{(2L - x + ut)}{\sqrt{4D_H t}}\right] \right\} \tag{27}$$

In dimensionless form,

$$\begin{aligned}
 A(\tilde{x}, \tilde{t}) = & \frac{1}{2} \operatorname{erfc} \left[\frac{\sqrt{\operatorname{Pe}} (\tilde{x} - \tilde{t})}{2 \sqrt{\tilde{t}}} \right] + \sqrt{\frac{\operatorname{Pe}}{\pi \tilde{t}}} \exp \left(-\frac{\operatorname{Pe} (\tilde{x} - \tilde{t})^2}{4 \tilde{t}} \right) \\
 & - \frac{1}{2} (1 + \operatorname{Pe} \tilde{x} + \operatorname{Pe} \tilde{t}) \exp(\operatorname{Pe} \tilde{x}) \operatorname{erfc} \left[\frac{\sqrt{\operatorname{Pe}} (\tilde{x} + \tilde{t})}{2 \sqrt{\tilde{t}}} \right] \\
 & + \sqrt{\frac{4 \operatorname{Pe}}{\pi \tilde{t}}} \left[1 + \frac{\operatorname{Pe}}{4} (2 - \tilde{x} + \tilde{t}) \right] \exp \left(\operatorname{Pe} - \frac{\operatorname{Pe} (2 - \tilde{x} + \tilde{t})^2}{4 \tilde{t}} \right) \\
 & - \operatorname{Pe} \left\{ \left[2 - \tilde{x} + \frac{3}{2} \tilde{t} + \frac{\operatorname{Pe}}{4} (2 - \tilde{x} + \tilde{t})^2 \right] \exp(\operatorname{Pe}) \operatorname{erfc} \left[\frac{\sqrt{\operatorname{Pe}} (2 - \tilde{x} + \tilde{t})}{2 \sqrt{\tilde{t}}} \right] \right\}
 \end{aligned} \tag{28}$$

Appendix 2: Verification of COMSOL

Figure 5 shows the verification of COMSOL numerical solution against the Brenner analytic solution with Robin–Neumann BCs (Brenner 1962), both in dimensionless units. The verification was performed for a conservative tracer and a partitioning tracer assuming equilibrium conditions. COMSOL model setup consists of a 1D length domain of $\tilde{x} = 1$, discretized in 50 intervals. Dimensionless time step discretization is $\Delta \tilde{t} = 1 \times 10^{-3}$. Péclet number used is 2, which corresponds to high dispersion. Dimensionless pulse time injected is $\tilde{t}_s = 0.2$. For the conservative tracer, the retardation factor is $R = 1$. For the equilibrium partitioning tracer, the retardation factor is $R = 1.5$, equivalent to assuming 20% remaining oil saturation $S_o = 0.2$, and a partitioning coefficient of $K = 2$.

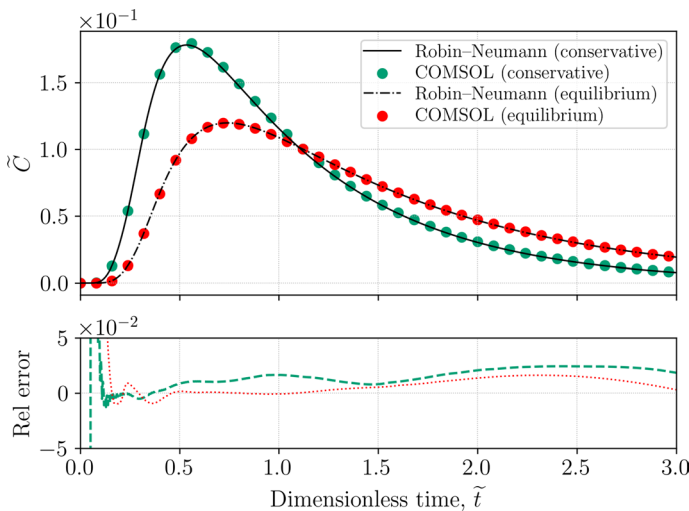


Fig. 5 Top: Dimensionless concentration histories of conservative and partitioning (equilibrium) tracer with Robin–Neumann boundary conditions obtained using an analytic solution by Brenner (black solid and dot-dashed lines) and numerical solutions by COMSOL (green and red circles). $\tilde{x} = 1$. $\tilde{t}_s = 0.2$. $\operatorname{Pe}_L = 2$. For the partitioning tracer, $S_o = 0.2$ and $K = 2$ ($R = 1.25$). Bottom: The relative error, in fraction, of the numerical solutions with respect to the analytic solutions

Appendix 3: Non-equilibrium Results (Pe = 100)

See Fig. 6.

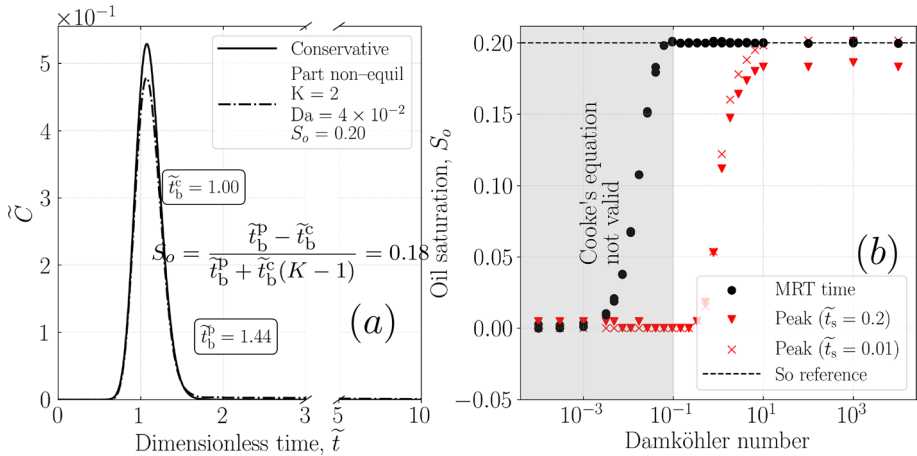


Fig. 6 **a** Dimensionless concentration histories of conservative and non-equilibrium partitioning tracers. $\tilde{x} = 1$, $Pe_L = 100$, and $\tilde{\tau}_s = 0.2$. For the partitioning tracer, $S_o = 0.2$ and $K = 2$ ($R = 1.5$). \tilde{t}_b^c and \tilde{t}_b^p are the calculated breakthrough times of the conservative and partitioning tracer, respectively. **b** Remaining oil saturation calculated with Cooke's equation under different Damköhler numbers using the non-equilibrium partitioning tracer model. Black filled circles are calculated using the mean residence time. Red triangles and crosses are calculated using the peak (mode) of the concentration distributions for $\tilde{\tau}_s = 0.2$ and $\tilde{\tau}_s = 0.01$, respectively. $K = 2$, reference oil saturation, $S_o = 0.2$, and $Pe_L = 100$

Appendix 4: Damköhler Number Estimation

The specific surface area of the oil–brine interface, a_v^i , has been estimated in the literature. Joekar-Niasar and Hassanizadeh (2012) obtain the dependence of fluid–fluid specific interfacial area from oil saturation in micromodels. Their range is 1–10 m^{-1} . Dastjerdi et al. (2024) found values of the order of hundreds m^{-1} from micromodels. Chatzis et al. (1983) demonstrated that in homogeneous Berea sandstone, experimental specific interfacial area is less than that values found in micromodel experiments or from theory predictions. Limestones are rather heterogeneous, which should increase the specific interfacial area. So, perhaps an estimate of 10–100 m^{-1} is reasonable. Another way to obtain a rough estimate is by using the specific surface area of the rock, a_v . Namely, the expression for specific interfacial area $a_v^i = \omega \cdot a_v \cdot S_o \cdot (1 - S_o) / \phi$ (m^{-1}) captures the general experimental trend in the cited manuscripts of the interfacial surface area being minimal at very low and very high oil saturations. In this expression, ω is an empirical coefficient that accounts for the distribution of oil and brine. We set ω equal to 0.5. In this case, the specific interfacial area is of the order of 1000 m^{-1} , a value that we used for our estimates. The specific interfacial area of large oil blobs or patches is probably smaller than the specific surface area because of the distribution of oil clusters. These arguments allow us to narrow down the range.

The molecular diffusion coefficient of the partitioning tracer in the oil phase could be measured in the laboratory. A simple estimate of the tracer diffusion coefficient in the oil

Table 2 Parameters to estimate Damköhler

Parameter	Lower bound	Upper bound
Specific interfacial area, a_v^i (m^{-1})	1000	100,000
Molecular diffusion of partitioning tracer, D_m^o ($\text{m}^2 \text{s}^{-1}$)	1×10^{-11}	1×10^{-9}
Mass transfer rate coefficient, α (s^{-1})	1×10^{-8}	1×10^{-4}
Length of the domain, L (m)	100	1000
Damköhler number, Da_m (-)	7×10^{-2}	7×10^3

Darcy velocity = 1.4×10^{-5} m/s. $\delta = 1$ m

phase is that of the Stokes–Einstein–Sutherland equation (Einstein 1905; Sutherland 1905; Smoluchowski 1906). Because of generally higher oil viscosities, a reasonable estimate is a factor of 10 lower than its diffusion coefficient in the water phase. For our analysis we used $1 \times 10^{-10} \text{ m}^2/\text{s}$.

Finally, perhaps the most difficult parameter to estimate is the average transverse characteristic dimension of oil patches. We believe that such a dimension should be measured in the units of rock REV. If oil displacement is efficient, the characteristic dimension of the remaining oil patches should be on the order of a few REVs. For example, during an efficient oil displacement from homogeneous rock, the size of the remaining oil patches is a few pore sizes, regardless of the displacement scale. However, for heterogeneous rocks, such as limestones, the remaining oil blob dimensions differ drastically from laboratory to field displacements. If the REV is unknown from the reservoir geological description, we can estimate REV based on the rock specific surface area. The characteristic dimension is $1/a_v$. We assume that for heterogeneous rocks, the REV dimension is at least 100–1000 times larger than the characteristic dimension of the rock to capture heterogeneity. For a typical limestone with $a_v = 10^4 \text{ m}^{-1}$, we find that REV is on the order of 0.1 m. Finally, the remaining blob size consists of a few REVs, so the value of 0.5 m is reasonable. On the other hand, in the field test analyzed, we find that $\text{Da}_m = 1.2$. This value for Da_m is obtained using the following parameters: $a_v^i = 1000 \text{ m}^{-1}$, $D_m^o = 1.75 \times 10^{-11} \text{ m}^2 \text{ s}^{-1}$, $\delta = 0.5 \text{ m}$.

Appendix 5: Field IPTT Modeling: Oil Cut Effect

In this section, we investigate the effect of the mobile oil on partitioning tracer arrival using a flow model with a constant oil cut of 4%. The test model assumes equilibrium between both mobile oil and water phases, and non-equilibrium between the mobile water phase and the stagnant oil phase. Figure 7 compares model concentration histories to results from the manuscript in Fig. 4. Only the non-equilibrium case for $K = 4$ is presented. The red dotted line corresponds to the non-equilibrium model from the manuscript (see Fig. 4b) and does not account for mobile oil (i.e. oil cut, $\text{OC} = 0\%$), $\text{Da}_m = 1.2$, and oil saturation (stagnant) $S_o = 0.2$. The green dot-dashed line assumes a total oil saturation of $S_o = 0.24$ that consists of 20.8% stagnant and 3.2% mobile oil. $\text{Da}_m = 1.2$ is also the same. The effect of the 4% oil cut on partitioning tracer is seen to be negligible.

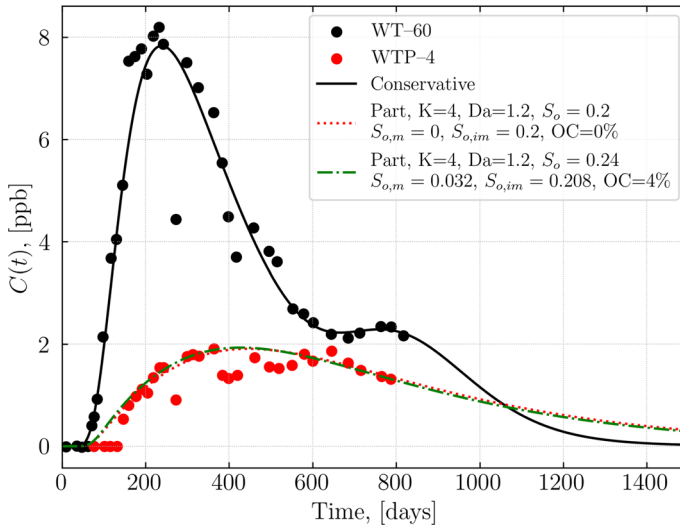


Fig. 7 Dimensional field concentration histories and models. The black filled circles represent the conservative tracer WT-60; red filled circles represent the partitioning tracer WTP-4 with $K = 4$. The red dotted line corresponds to the model for non-equilibrium partitioning tracers $K = 4$, as shown in Fig. 4b with zero oil cut (OC). The green dot-dashed line corresponds to the model with 4% oil cut, assuming equilibrium between mobile water and mobile oil phases, and non-equilibrium between the mobile water and stagnant oil phases. The legend values of S_o correspond to the total oil saturation, $S_{o,m}$ to the mobile oil saturation, $S_{o,im}$ to the immobile oil saturation

Acknowledgements The authors want to thank Prof. Hussein Hoteit for the useful discussion and suggestions. The research reported in this publication has been funded by KAUST through baseline research funds to Prof. Tadeusz Patzek.

Funding Open access publishing provided by King Abdullah University of Science and Technology (KAUST).

Declarations

Funding The research reported in this publication was funded by KAUST through baseline research funds BAS/1378/01/01 to Prof. Tadeusz Patzek.

Conflict of interest The authors have no Conflict of interest to declare that are relevant to the content of this article.

Author contribution Conceptualization contributed by all authors; methodology contributed by Samuel Fontalvo, Maxim Yutkin; formal analysis and investigation contributed by Samuel Fontalvo, Maxim Yutkin; writing—original draft preparation contributed by Samuel Fontalvo, Maxim Yutkin; writing—review and editing contributed by Majid Hassanizadeh, Clayton Radke, Tadeusz Patzek; funding acquisition contributed by Tadeusz Patzek; supervision contributed by Tadeusz Patzek.

Open Access This article is licensed under a Creative Commons Attribution 4.0 International License, which permits use, sharing, adaptation, distribution and reproduction in any medium or format, as long as you give appropriate credit to the original author(s) and the source, provide a link to the Creative Commons licence, and indicate if changes were made. The images or other third party material in this article are included in the article's Creative Commons licence, unless indicated otherwise in a credit line to the material. If material is not included in the article's Creative Commons licence and your intended use is not

permitted by statutory regulation or exceeds the permitted use, you will need to obtain permission directly from the copyright holder. To view a copy of this licence, visit <http://creativecommons.org/licenses/by/4.0/>.

References

- Abbaszadeh-Dehghani, M., Brigham, W.E.: Analysis of Well-to-Well Tracer Flow to Determine Reservoir Layering. Society of Petroleum Engineers, Calgary (1984). <https://doi.org/10.2118/10760-PA>
- Berkowitz, B., Emmanuel, S., Scher, H.: Non-fickian transport and multiple-rate mass transfer in porous media. *Water Resour. Res.* **44**, 1–16 (2008). <https://doi.org/10.1029/2007WR005906>
- Brenner, H.: The diffusion model of longitudinal mixing in beds of finite length. Numerical values. *Chem. Eng. Sci.* **17**, 3937–3947 (1962). [https://doi.org/10.1016/0009-2509\(62\)85002-7](https://doi.org/10.1016/0009-2509(62)85002-7)
- Brigham, W.E., Smith, D.H.: Prediction of Tracer Behavior in Five-Spot Flow. Society of Petroleum Engineers, Calgary (1965). <https://doi.org/10.2118/1130-MS>
- Carslaw, H.S., Jaeger, J.C.: *Conduction of Heat in Solids*. Clarendon Press, Oxford (1959)
- Chatzis, I., Morrow, N.R., Lim, H.T.: Magnitude and Detailed Structure of Residual Oil Saturation. Society of Petroleum Engineers, Calgary (1983). <https://doi.org/10.2118/10681-PA>
- Cleary, R.W., Adrian, D.D.: Analytical Solution of the Convective–Dispersive Equation for Cation Adsorption in Soils. *Soil Science Society of America, Madison* (1973). <https://doi.org/10.2136/sssaj1973.03615995003700020014x>
- Coats, K.H., Smith, B.D.: Dead-End Pore Volume and Dispersion in Porous Media. Society of Petroleum Engineers, Calgary (1964). <https://doi.org/10.2118/647-PA>
- Cooke, C.E.: *Method of Determining Fluid Saturations in Reservoirs*, p. 3590923. Esso Production Research Company, Spring (1971)
- Danckwerts, P.V.: Continuous flow systems. *Chem. Eng. Sci.* (1953). [https://doi.org/10.1016/0009-2509\(53\)80001-1](https://doi.org/10.1016/0009-2509(53)80001-1)
- Dastjerdi, S.V., Karadimitriou, N., Hassanizadeh, S.M., Steeb, H.: Formation of common preferential two-phase displacement pathways in porous media. *Water Resour. Res.* (2024). <https://doi.org/10.1029/2024WR037266>
- Deans, H.A.: A Mathematical Model for Dispersion in the Direction of Flow in Porous Media. Society of Petroleum Engineers, Calgary (1963). <https://doi.org/10.2118/493-PA>
- Dwarakanath, V., Deeds, N., Pope, G.A.: Analysis of partitioning interwell tracer tests. *Environ. Sci. Technol.* (1999). <https://doi.org/10.1021/es990082v>
- Einstein, A.: Über die von der molekularkinetischen theorie der wärme geforderte bewegung von in ruhenden flüssigkeiten suspendierten teilchen. *Ann. Phys.* (1905). <https://doi.org/10.1002/andp.19053220806>
- Genunchten, M.V.: Analytical solutions for chemical transport with simultaneous adsorption, zero-order production and first-order decay. *J. Hydrol.* (1981). [https://doi.org/10.1016/0022-1694\(81\)90214-6](https://doi.org/10.1016/0022-1694(81)90214-6)
- Genunchten, M.V., Parker, J.C.: Boundary Conditions for Displacement Experiments Through Short Laboratory Soil Columns. *Soil Science Society of America, Madison* (1984). <https://doi.org/10.2136/sssaj1984.03615995004800040002x>
- Genunchten, M.V., Wierenga, P.J.: Mass Transfer Studies in Sorbing Porous Media I. Analytical Solutions. *Soil Science Society of America, Madison* (1976). <https://doi.org/10.2136/sssaj1976.03615995004000040011x>
- Genunchten, M.V., Wierenga, P.J.: Solute Dispersion Coefficients and Retardation Factors. *American Society of Agronomy - Soil Science Society of America, Madison* (1986). <https://doi.org/10.2136/sssabookser5.1.2ed.c44>
- Genunchten, M.V., Leij, F.J., Skaggs, T.H., Toride, N., Bradford, S.A., Pontedeiro, E.M.: Exact analytical solutions for contaminant transport in rivers I. The equilibrium advection-dispersion equation. *J. Hydrol. Hydromech.* **61**, 146 (2013)
- Golz, W.J.: On the convection–dispersion equation for a finite domain: third-type boundaries as a necessary condition of the conservation law. *arXiv* (2004) <https://doi.org/10.48550/arXiv.math/0410279>
- Hartvig, S., Huseby, O., Yasin, V., Ogezi, O., Ernst, B., Reimann, S., Leonhardt, B.: Use of a New Class of Partitioning Tracers to Assess EOR and IOR Potential In the Bockstedt Field. *European Association of Geoscientists & Engineers, Bunnik* (2015). <https://doi.org/10.3997/2214-4609.201412118>
- Huseby, O., Hartvig, S., Jevanord, K., Dugstad, O.: Assessing EOR Potential From Partitioning Tracer Data. Society of Petroleum Engineers, Calgary (2015). <https://doi.org/10.2118/172808-MS>

- Joekar-Niasar, V., Hassanizadeh, S.M.: Uniqueness of specific interfacial area-capillary pressure-saturation relationship under non-equilibrium conditions in two-phase porous media flow. *Transp. Porous Media* (2012). <https://doi.org/10.1007/s11242-012-9958-3>
- Khirevich, S., Patzek, T.W.: Three-dimensional simulation of tracer transport dynamics in formations with high-permeability channels or fractures: estimation of oil saturation. *Phys. Fluids* (2019). <https://doi.org/10.1063/1.5120415>
- Kreft, A., Zuber, A.: On the physical meaning of the dispersion equation and its solutions for different initial and boundary conditions. *Chem. Eng. Sci.* **33**, 1471–1480 (1978). [https://doi.org/10.1016/0009-2509\(78\)85196-3](https://doi.org/10.1016/0009-2509(78)85196-3)
- Lapidus, L., Amundson, N.: Mathematics of adsorption in beds. The effect of longitudinal diffusion in ion exchange and chromatographic columns. *J. Phys. Chem.* **56**, 4 (1952). <https://doi.org/10.1021/j150500a014>
- Levenspiel, O.: *Chemical Reaction Engineering*. Wiley, Hoboken (1999)
- Levenspiel, O., Smith, W.K.: Notes on the diffusion-type model for the longitudinal mixing of fluids in flow. *Chem. Eng. Sci.* (1979). [https://doi.org/10.1016/0009-2509\(96\)81816-1](https://doi.org/10.1016/0009-2509(96)81816-1)
- Lindstrom, F.: A mathematical model simulating mass transport of chemicals in saturated porous media. Thesis (1969). <http://hdl.handle.net/1957/17211>
- Lindstrom, F., Rizwanul, H., Freed, V., Boersma, L.: Theory on the movement of some herbicides in soils: linear diffusion and convection of chemicals in solids. *Environ. Sci. Technol.* **1**, 561–565 (1967). <https://doi.org/10.1021/es60007a001>
- Maroongroge, V.: Modeling and application of tracers for reservoir characterization. Thesis, University of Texas at Austin (1994). <https://doi.org/10.26153/tsw/7654>
- Niessner, J., Hassanizadeh, S.M.: Modeling kinetic interphase mass transfer for two-phase flow in porous media including fluid–fluid interfacial area. *Transp. Porous Media* **80**, 329–344 (2009). <https://doi.org/10.1007/s11242-009-9358-5>
- Nkedi-Kizza, P., Biggar, J.W., Selim, H.M., Genuchten, M.V., Wierenga, P.J., Davidson, J.M., Nielsen, D.R.: On the equivalence of two conceptual models for describing ion exchange during transport through an aggregated oxisol. *Water Resour. Res.* (1984). <https://doi.org/10.1029/WR020i008p01123>
- Novakowski, K.: An evaluation of boundary conditions for one-dimensional solute transport. *Water Resour. Res.* **28**, 2411–2423 (1992). <https://doi.org/10.1029/92WR00592>
- Parker, J.C.: Analysis of Solute Transport in Column Tracer Studies. Soil Science Society of America, Madison (1984). <https://doi.org/10.2136/sssaj1984.03615995004800040005x>
- Pearson, J.R.: A note on the “danckwerts” boundary conditions for continuous flow reactors. *Chem. Eng. Sci.* **10**, 281–284 (1959). [https://doi.org/10.1016/0009-2509\(59\)80063-4](https://doi.org/10.1016/0009-2509(59)80063-4)
- Raimondi, P., Torcaso, M.A.: Mass Transfer Between Phases in a Porous Medium: A Study of Equilibrium. Society of Petroleum Engineers, Calgary (1965). <https://doi.org/10.2118/959-PA>
- Rao, P.S.C., Rolston, D.E., Jessup, R.E., Davidson, J.M.: Solute Transport in Aggregated Porous Media: Theoretical and Experimental Evaluation. Soil Science Society of America, Madison (1980a). <https://doi.org/10.2136/sssaj1980.03615995004400060003x>
- Rao, P.S.C., Jessup, R.E., Davidson, J.M., Kilcrease, D.P.: Experimental and Mathematical Description of Nonadsorbed Solute Transfer by Diffusion in Spherical Aggregates. Soil Science Society of America, Madison (1980b). <https://doi.org/10.2136/sssaj1980.03615995004400040004x>
- Sanni, M., Al-Abbad, M., Kokal, S., Hartvig, S., Huseby, O., Jevanord, K.: A Field Case Study of Inter-well Chemical Tracer Test. Society of Petroleum Engineers, Calgary (2015). <https://doi.org/10.2118/173760-MS>
- Sanni, M., Al-Abbad, M., Kokal, S., Dugstad, O., Hartvig, S., Huseby, O.: Pushing the Envelope of Residual Oil Measurement: A Field Case Study of a New Class of Inter-well Chemical Tracers. Society of Petroleum Engineers, Calgary (2016). <https://doi.org/10.2118/181324-MS>
- Sanni, M., Al-Abbad, M., Kokal, S., Ali, R., Zefzafy, I., Hartvig, S., Huseby, O.: Reservoir Description Insights from an Inter-well Chemical Tracer Test. Society of Petroleum Engineers, Calgary (2017). <https://doi.org/10.2118/188060-MS>
- Shook, G.M.: A systematic method for tracer test analysis: an example using Beowawe tracer data. In: *Geothermal Reservoir Engineering* (2005)
- Shook, G.M., Pope, G.A., Asakawa, K.: Determining Reservoir Properties and Flood Performance from Tracer Test Analysis. Society of Petroleum Engineers, Calgary (2009). <https://doi.org/10.2118/124614-MS>
- Skopp, J., Warrick, W.: A Two-Phase Model for the Miscible Displacement of Reactive Solutes in Soils. Soil Science Society of America, Madison (1974). <https://doi.org/10.2136/sssaj1974.03615995003800040012x>
- SLB glossary: breakthrough. <https://glossary.slb.com/en/terms/b/breakthrough>

- Smoluchowski, M.V.: Zur kinetischen theorie der brownischen molekularbewegung und der suspensionen. *Ann. Phys.* (1906). <https://doi.org/10.1002/andp.19063261405>
- Sutherland, W.: A dynamical theory of diffusion for non-electrolytes and the molecular mass of albumin. *Lond. Edinb. Dublin Philos. Mag. J. Sci.* (1905). <https://doi.org/10.1080/14786440509463331>
- Tang, J.S., Harker, B.: Interwell tracer test to determine residual oil saturation in a gas-saturated reservoir. Part I: theory and design. *J. Can. Pet. Technol.* (1991a). <https://doi.org/10.2118/91-03-08>
- Tang, J.S., Harker, B.: Interwell tracer test to determine residual oil saturation in a gas-saturated reservoir. Part II: field applications. *J. Can. Pet. Technol.* (1991b). <https://doi.org/10.2118/91-04-01>
- Viig, S.O., Juilla, H., Renouf, P., Kleven, R., Krognnes, B., Dugstad, O., Huseby, O.: Application of a New Class of Chemical Tracers to Measure Oil Saturation in Partitioning Interwell Tracer Tests. Society of Petroleum Engineers, Calgary (2013). <https://doi.org/10.2118/164059-MS>
- Yutkin, M.P., Radke, C.J., Patzek, T.W.: *Chemical Compositions in Modified Salinity Waterflooding of Calcium Carbonate Reservoirs: Experiment*. Springer, Berlin (2022). <https://doi.org/10.1007/s11242-020-01517-7>

Publisher's Note Springer Nature remains neutral with regard to jurisdictional claims in published maps and institutional affiliations.

Authors and Affiliations

Samuel D. Fontalvo¹  · Maxim P. Yutkin¹ · S. Majid Hassanizadeh^{2,3} · Clayton J. Radke⁴ · Tadeusz W. Patzek¹

✉ Samuel D. Fontalvo
samuel.fontalvoguzman@kaust.edu.sa

Maxim P. Yutkin
maxim.yutkin@kaust.edu.sa

S. Majid Hassanizadeh
s.m.hassanizadeh@uu.nl

Clayton J. Radke
radke@berkeley.edu

Tadeusz W. Patzek
tadeusz.patzek@kaust.edu.sa

¹ King Abdullah University of Science and Technology, 23955 Thuwal, Saudi Arabia

² SimTech, Stuttgart University, 70569 Stuttgart, Germany

³ Utrecht University, 80125 Utrecht, The Netherlands

⁴ University of California, Berkeley, CA 94720, USA